Energy-loss straggling of helium projectiles at low kinetic energies

Gunther Andersson*
Wilhelm-Ostwald-Institute for Physical and Theoretical Chemistry, Leipzig University, Linnestrasse 3, 04103 Leipzig, Germany
(Received 8 September 2006; published 16 March 2007)

Concentration depth profiles at liquid surfaces can be determined by means of neutral impact collision ion scattering spectroscopy. The energy resolution of the spectra is influenced by the energy loss straggling of the projectiles. Energy loss straggling is a measure of the width of the energy loss distribution of particles passing through matter. Knowledge of the energy loss straggling is especially important for determining concentration depth profiles of aqueous surfaces. Here it is shown that the energy loss in the gas phase and the energy loss distribution can be determined with a series of spectra taken at different vapor pressures of the aqueous solution. The projectiles used are 3 keV helium ions. The gas phase causes a shift of the spectra to lower energies and a broadening of the structure due to energy loss straggling. Both the energy loss in the gas phase and the energy loss straggling must be gauged in order to determine concentration depth profiles quantitatively. Knowledge of the energy loss distribution can be used to determine accurate concentration depth profiles by means of deconvolution.

DOI: 10.1103/PhysRevA.75.032901 PACS number(s): 34.50.Bw, 68.03.−g

I. INTRODUCTION

Liquid surfaces play an important role in a great variety of areas such as atmospheric research, biological membranes and the adsorption of surfactants. A fundamental understanding of liquid surfaces requires a knowledge of their molecular structure. For a long time the investigation of liquid surfaces was limited to the measurement of macroscopic properties such as the surface potential or the surface tension in combination with thermodynamic concepts.

In the past decades some methods have been developed to directly investigate the molecular structure of liquid surfaces: X-ray reflectivity (XR) [1], neutron reflectivity (NR) [2–4], nonlinear optical (NLO) methods [5,6], molecular beam techniques [7], angle resolved x-ray photoelectron spectroscopy (ARXPS) [8], metastable induced electron spectroscopy (MIES) [9], and neutral impact collision ion scattering spectroscopy (NICISS) [10].

The concentration depth profiles of the constituents are important features of the region near the liquid surface. Besides the reflectivity methods XR and NR only ARXPS and NICISS can be used to determine concentration depth profiles. With NICISS, concentration depth profiles can be determined with a depth resolution of a few Å [10].

Energetic ions and neutral atoms lose energy on their passage through matter by small angle scattering and electronic excitations. The slowing down process is accompanied by a spreading of the projectile energy which is due to the statistical fluctuations in the number of energy loss processes. Thus a monoenergetic beam of particles will have a distribution of kinetic energies after their passage through matter. The first moment of this distribution gives the mean energy loss and is called stopping power [11]. The nuclear stopping power refers to the slowing down by multiple small angle scattering events and the electronic stopping power refers to the electronic excitations. The second moment gives a measure of the width of the energy loss distribution [11] and is called energy loss straggling. The energy loss straggling is divided into a nuclear part, which is due to the statistics of the small angle scattering events, and the electronic energy loss straggling [12,13]. In a backscattering experiment there is an additional contribution to the energy distribution of the detected projectiles. The multiple small angle scattering events causes the blurring of the backscattering angle. The blurring of the backscattering angle itself also contributes to the broadening of the measured energy loss distribution. This effect should be considered separately from the energy loss straggling.

The energy resolution of a NICIS spectrum and hence the resolution of the concentration depth profiles is—apart from the resolution of the spectrometer—determined by the distribution of inelastic energy losses during the backscattering process and the energy loss straggling of the projectiles. The distribution of inelastic energy losses during the backscattering process can be determined by gas phase experiments [14]. The energy loss straggling of the projectiles is subject of this paper. Energy loss straggling of projectiles with high kinetic energies (~MeV) has been experimentally determined [15–18]. The distribution function of the energy losses has been calculated by solving the transport equation [19,20]. For the calculation of the energy loss distribution it is required to know the probability function of an energy loss. The function is known for high energy particles [21]. If the maximum possible energy transfer in a single energy loss process is not small compared to the total energy loss of a projectile, the energy loss distribution will be asymmetric [17].

Experimental results at low energies, however, are rare. In some cases the results are strongly affected by the energy resolution of the spectrometer [22]. Since the probability function of an energy loss is not known for low energies, the energy loss distribution cannot be calculated following the approach of Landau and Vavilov [19,20].

The purpose of this paper is to show, how the distribution of energy losses of projectiles passing through matter and

*Electronic address: g.andersson@uni-leipzing.de

thus the energy loss straggling can be experimentally determined for low kinetic energies by means of NICISS.

NICISS is used to determine concentration depth profiles of soft matter surfaces [10]. Determining the energy loss straggling is an important problem in the investigation of aqueous surfaces. In contrast to the investigation of solvents with low vapor pressure like formamide, the energy and thus the depth resolution of the NICIS spectra is affected by the gas phase in front of the aqueous surface. For this reason, aqueous surfaces have not yet been investigated with this method, although water is the most important solvent of all. As an example, a question that currently attracts a lot of interest is whether or not inorganic ions like iodide being constituents of inorganic salts are present at liquid surfaces in a concentration that exceeds the bulk concentration [23–26] in spite of their surface excess being negative. Recently Hemminger *et al.* showed that it is possible to investigate saturated aqueous solutions at low temperatures with x-ray photoelectron spectroscopy (XPS) [27,28], a technique also carried out in vacuum. Unfortunately, they were not able to show quantitative concentration depth profiles.

II. EXPERIMENT

The NICISS setup and the method itself is described in detail in [29]. The target is bombarded with a pulsed beam of inert gas ions—mostly helium ions—with a kinetic energy of several keV. The energy of the projectiles backscattered from the atoms in the target is determined by their time-of-flight (TOF) from the target to the detector. The scattering angle used is 168° and the length of the TOF path is about 1.24 m. The time resolution can be estimated from the photon peak in the spectra and is 10 ns for the experiments shown here. The projectiles lose energy during the backscattering process and the energy transfer depends on the mass of the target atom. Additionally, the projectiles lose energy on their trajectory through the bulk due to small angle scattering of the projectile and electronic excitations of the molecules that constitute the target. The magnitude is proportional to the depth of the target atom. The depth that can be investigated by this method is limited by the blurring of the scattering angle due to multiple small angle scattering events. At an energy of 5 keV the maximum depth which can be investigated is about 300 Å. The dose of the He ions in a typical NICISS experiment investigating liquid surfaces is about 10^{10} ions/cm^2. Thus damage of the surface and the influence of the impinging ions on the surface structure can be neglected.

The method to create the liquid surface in the vacuum is described in detail in [29]. A reservoir in the vacuum chamber is filled with the liquid. A disk is immersed into the liquid and is rotated by a motor. As a result a thin lamella of the liquid develops on the disk. Due to the high vapor pressure of water, the target has been modified for the investigation of aqueous surfaces. The target is placed in a closed housing with a small aperture in front of the disk. The aperture has a diameter of 1.0 mm. The ion beam analysis is carried out through the aperture. The construction of the target is described in detail in [30].

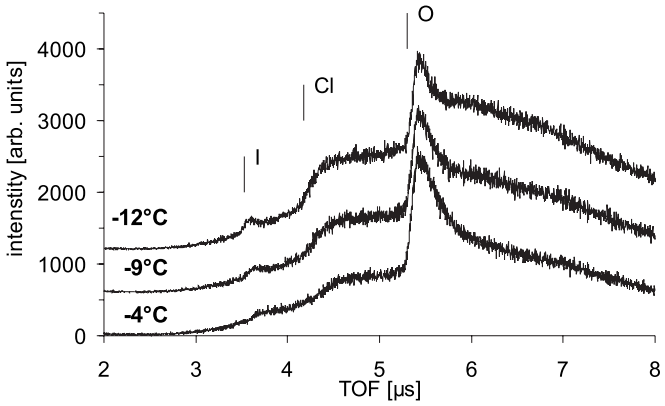

FIG. 1. TOF spectra of a solution of 0.01mBu$_4$NI and 2.5mLiCl in water at different temperatures. The spectra are offset for clarity. The spectra show structures due to iodide, chloride, and oxygen. In the spectra no signal of carbon can be identified. Lithium cannot be identified due to its low cross section.

A solution of 0.01mBu$_4$NI and 2.5mLiCl in water was investigated. Bu$_4$NI and LiCl were purchased from Aldrich. LiCl was added to the solution in order to lower the freezing point of the solution. The measurements were carried out with 3 keV helium ions. The detector efficiency was determined by measuring the spectra of a solution of NaI in formamide with a fixed bulk concentration at different primary energies. After correcting the spectra for the cross section, the detector efficiency can be determined by assuming that the concentration depth profile of the solute in the bulk is constant. The detector efficiency was taken into account in the data evaluation.

III. RESULTS

A. Measurements

In Fig. 1 TOF spectra are shown of a solution of 0.01mBu$_4$NI and 2.5mLiCl in water at different temperatures. The vapor pressure of each solution is given in Table I. The vapor pressure is calculated from the vapor pressure of pure water [31], taking into account the activity. The vapor pressure was measured in [31] with the static method using a pressure gauge developed by Rayleigh [32]. The activities are calculated from the freezing point depression given in [33]. Structures due to oxygen, chloride, and iodide can be identified in the spectra. The onsets of the structures on the

TABLE I. Vapor pressures of the solutions at the various temperatures calculated according to the activity of the LiCl.

Temperature (°C)	Vapor pressure (mbar)
−13.2	2.0
−12	2.1
−10.5	2.4
−9	2.7
−7	3.2
−4	4.0

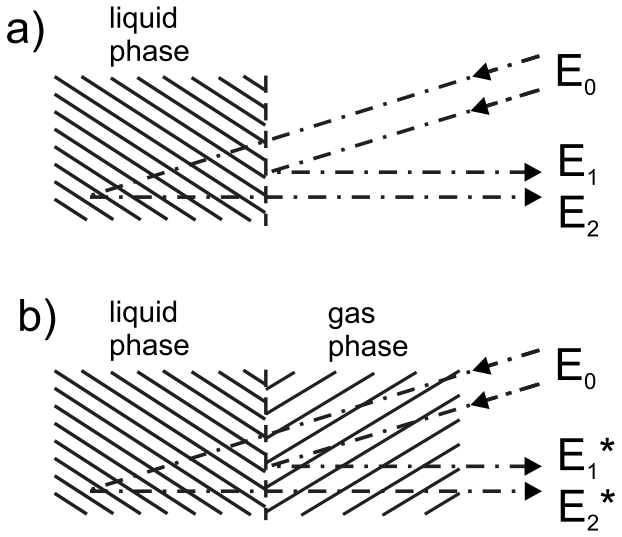

FIG. 2. Scheme of the influence of the gas phase on the energy loss of the backscattered projectiles.

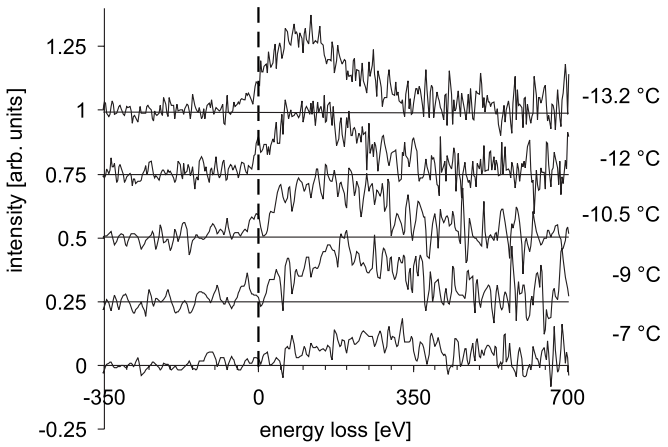

FIG. 3. Energy loss spectra of iodide at different temperatures. An offset is added to the spectra in order to separate the spectra in the diagram. From all the spectra the center of gravity of the peak in the spectrum measured at −7 °C is most difficult to determine. Therefore the error bars of the points in Fig. 4 attributed to this spectrum have the largest error bars.

TOF scale are indicated with bars. The structures can be separated from the spectra as described in [34] and converted into the energy loss scale. The energy loss is the difference between the energy of a projectile backscattered from a specific element being in the outermost layer and the measured energy of the projectile. The energy of a projectile backscattered from the outermost layer is gauged with gas phase spectra [14].

The influence of the gas phase in front of the liquid surface on the energy of the backscattered projectiles is sketched in Fig. 2. The energy of projectiles backscattered from a specific element in the outermost layer of the liquid phase is E_1, in the case that the gas phase can be neglected as shown in Fig. 2(a). E_1 is determined by gas phase experiments [14]. The energy of a projectile backscattered from the depth d is given by

$$E_2 = E_1 - \Delta E_{\mathrm{liq}}, \quad \Delta E_{\mathrm{liq}} = \Delta E_{\mathrm{liq}}(d), \tag{1}$$

where ΔE_{liq} is the energy loss in the bulk of the liquid. The energy of projectiles backscattered from a specific element in the outermost layer of the liquid phase is E_1^*, in the case that the gas phase cannot be neglected as shown in Fig. 2(b). The energy E_1^* is given by

$$E_1^* = E_1 - \Delta E_{\mathrm{gas}}, \tag{2}$$

where ΔE_{gas} is the energy loss in the gas phase in front of the liquid surface. The energy of a projectile backscattered from the depth d of the liquid phase is calculated analogous to Eq. (2), taking into account that the stopping power depends on the energy of the projectile. As a consequence the energy loss spectrum of an element that is a constituent only of the liquid phase is shifted to a greater energy loss when the density of the gas phase in front of the target increases.

The shape of the oxygen step as shown in Fig. 1 needs separate consideration. The oxygen step originates from projectiles backscattered from water in the gas phase in front of the liquid phase and from the liquid phase. In the case that the influence of the gas phase cannot be neglected, the part of the energy loss spectrum close to the onset of the step is due to projectiles backscattered from the gas phase. Since the mole fraction of water in the gas phase and in the liquid phase differs only by a few percent, the oxygen step is expected to be approximately constant. However, the oxygen step in Fig. 1 shows a broad maximum at the onset of the step. The reason for the appearance of the broad maximum is that in the experiments shown here the area hit by the ion beam did not coincide fully with the opening of the aperture in front of the target. This is due to the fact that it is very difficult in the current setup to align the ion beam with the center of the aperture. Thus the area of the gas phase hit by the ion beam in front of the aperture is slightly greater than that of the gas phase and liquid phase behind the aperture. Consequently the count rate of projectiles backscattered from oxygen is greater for the gas phase in front of the aperture than the count rate of projectiles backscattered from oxygen behind the aperture. This causes the broad maximum at the onset of the oxygen step. In the case of a poorly adjusted ion beam, a carbon step also appears in the spectra since the aperture is covered with graphite. However, there is no influence on the other structures of the spectra if the ion beam is not perfectly directed to the opening of the aperture.

In Fig. 3 the energy loss spectra of helium backscattered from iodide are shown. The gauging of the energy loss scale has been determined by the gas phase spectrum of diiodomethane as described in [14]. Iodide, which is the anion of the ionic surfactant, adsorbs at the liquid surface and causes a peak in the spectra. Chloride has a smaller ionic radius than iodide and a greater solvation shell. As a consequence, chloride has a lower tendency than iodide to adsorb at the surface [35] as the counter ion of Bu_4N^+. Consequently there is no peak at the onset of the chloride step. With increasing temperature the maximum of the iodide spectra shifts to a greater energy loss and the spectra become broader. The shift is caused by the increasing energy loss of

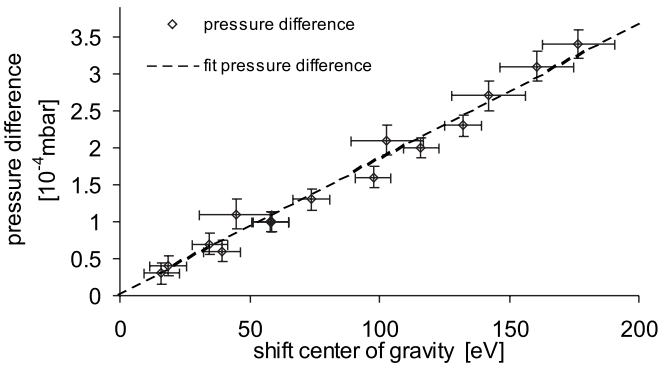

FIG. 4. The difference of the pressure in the target chamber during the measurement of each two spectra is shown as the function of the difference of the center of gravity of the peaks in the respective energy loss spectra.

the projectiles in the gas phase in front of the target and increases with the increasing temperature. The broadening is due to the energy loss straggling and also increases with the increasing density of the gas phase in front of the target.

B. Mean energy loss in the gas phase

The aim of the data evaluation is to quantitatively determine both the mean energy loss of the projectiles in the gas phase in front of the surface and the energy loss straggling. Determining the mean energy loss of the projectiles in the gas phase is required for gauging the zero of the depth scale of the liquid phase with respect to the gas phase. The first step in the evaluation of the data is to determine the mean energy loss of the projectiles in the gas phase at different temperatures. Bu_4NI has a high surface activity in water and the by far greatest fraction of intensity of the helium projectiles backscattered from iodide is found in the peak. Thus the shift of the iodide spectra due to the increasing density of the gas phase can be identified with the mean energy loss in the gas phase and calculated from the shift of the center of gravity of the energy loss spectrum of iodide. The center of gravity of the energy loss spectrum i is calculated by

$$\overline{E_i} = \frac{\int_{E_b}^{E_a} E I_i(E) dE}{\int_{E_b}^{E_a} I_i(E) dE}, \tag{3}$$

where $\overline{E_i}$ is the center of gravity of the peak i, $I_i(E)$ is the energy loss spectrum i, E is the energy loss and E_a and E_b are reasonable boundaries. Here E_a is chosen as -350 eV and E_b as 800 eV. With this procedure, it is assumed that the shape of the concentration depth profile of iodide does not change significantly with the temperature. For each two spectra, the difference between the respective pressures in the target chamber during the measurements are calculated. These differences are shown in Fig. 4 as function of the difference between the centers of gravity of the respective peaks in the energy loss spectra. It can be assumed that the pressure in the target chamber changes linearly with the density in the gas phase in front of the target, since the gas in the target chamber originates almost only from the target itself. It is found that the pressure difference is proportional to the shift of the peaks. From the linear fit the energy loss of the projectiles in the gas phase at a given pressure or temperature can be determined. Moreover, the stopping cross section of the helium projectiles in water vapor can be estimated to be $12(+6/-3)$ eV/(10^{15} molecules cm^2). The large error originates from the uncertainty in measuring the distance between the liquid surface and the aperture in front of the target in the current setup. In comparison, the stopping cross section calculated by using Bragg's rule [36] and the extrapolated data from [37] yield a value of 9.6 eV/(10^{15} molecules cm^2).

C. Energy loss distribution

In the second step of the data evaluation the energy loss straggling of the projectiles must be determined. Often a Gaussian curve seems to be suitable to describe the energy loss distribution and is assumed frequently for higher energies [38,39]. However, the disadvantage of a Gaussian curve is that its intensity ranges from minus infinity to plus infinity. To use a Gaussian curve for the fit procedure would mean that the projectiles could even significantly gain energy by passing through matter. This is not reasonable. The fact that the energy losses are restricted to values greater than zero implies that the energy loss distribution is asymmetric. Asymmetric distributions of the energy losses are observed [40] and attributed to thickness fluctuations. However, even in gas phase experiments measured at higher temperatures an asymmetric distribution can be observed with the broader part at the low energy side [39].

D. Fit of the energy loss distribution

The energy loss straggling is determined by seeking a suitable curve that is used for the convolution of a spectrum measured at a lower pressure (lower temperature) to fit a spectrum measured at a higher pressure (higher temperature). Assuming that the straggling in a given layer is independent from the straggling in the previous layers, we are seeking for a single distribution that is specific for projectiles passing through a layer with a specific amount of matter. This distribution is specific for a given mean energy loss. The energy distribution of the projectiles after passing through the layer is calculated by convoluting the energy distribution of the projectiles before passing through the layer with the energy loss distribution for the single layer. The energy loss straggling of the projectiles after passing through several layers, each with the same amount of matter, is calculated by a consecutive convolution where the number of convolutions is equal to the number of layers.

The spectrum at a given temperature was convoluted to fit the spectra at higher temperatures. All spectra at higher temperatures were fitted at the same time where the number of convolutions to fit a specific spectrum is given by the difference of the mean energy losses in the gas phase of the convoluted and the fitted spectrum. The difference in mean energy loss in the gas phase between two spectra was

calculated from the differences of the center of gravity of the spectrum at the lower temperature and the fitted spectrum (see Fig. 4). The center of gravity of a peak in an energy loss spectrum was calculated by Eq. (3).

For practical reasons the amount of water vapor in the single layer and thus the mean energy loss in the layer was chosen in such a way that the integral multiple of the mean energy loss in the single layer would be as close as possible to all the differences between the center of gravity of the energy loss spectra. In other words, the value of E_{sl}, i.e., the energy loss in the single layer, is determined such that the quantity Δ with

$$\Delta = \sum_{i<j} \sum_{j} \Delta_{ij} = \sum_{i<j} \sum_{j} \frac{[n_{ij}E_{sl} - (\overline{E_j} - \overline{E_i})]}{(\overline{E_j} - \overline{E_i})} \tag{4}$$

shall be a minimum, where $\overline{E_i}$ is calculated with Eq. (3) and $\overline{E_i} > \overline{E_j}$. The n_{ij} are the numbers of consecutive convolutions. The energy loss distribution in a single layer was chosen according to this criterion to yield E_{sl}=8.3 eV with each Δ_{ij} less than 10%. The value of 8.3 eV has no physical meaning but is chosen to enable the consecutive convolution. Since the density of the water vapor in front of the target as function of the distance to the liquid surface is not constant, the spatial thickness of the single layers are not constant but increasing with the distance to the liquid surface. By applying this convolution procedure, it is assumed that the energy loss and the energy loss straggling in each layer is independent from those in the other layers. This procedure is supported by the statistical nature of the slowing down process and by the fact that the energy loss in the water vapor is small compared to the kinetic energy of the projectile.

The fitting was carried out with a program based on the genetic algorithm. The program is similar to that described in [10]. In our fit procedure the intensities of the energy loss distribution in a single layer were chosen as the fit parameters. The advantage in choosing the intensities themselves as fit parameters is that our procedure is not restricted to a specific mathematical form of the function. In the present case, the side conditions in the fitting procedure are that the energy loss distribution in a single layer does not become too large (avoiding strong scattering of the intensities) and that the mean energy loss given by the energy loss distribution is close to the measured energy loss.

Several fits are shown in Fig. 5. They are reasonable within the statistics of the experiment. The energy loss distribution in a single layer is shown in Fig. 6. The curve is a weighted average of four different curves, each used to convolute the spectra at −13.2 °C, −12 °C, −10.5 °C, and −9 °C to fit the spectra measured at the higher temperature than the convoluted spectrum (five spectra have been fitted by convoluting the spectrum measured at −13.2 °C, four spectra by convoluting the spectrum measured at −12 °C and so on). The error bars are calculated from the differences between the four curves.

The energy loss distributions for several layers are shown in Fig. 7. They are calculated by a consecutive convolution of a delta function with the energy loss distribution in a single layer.

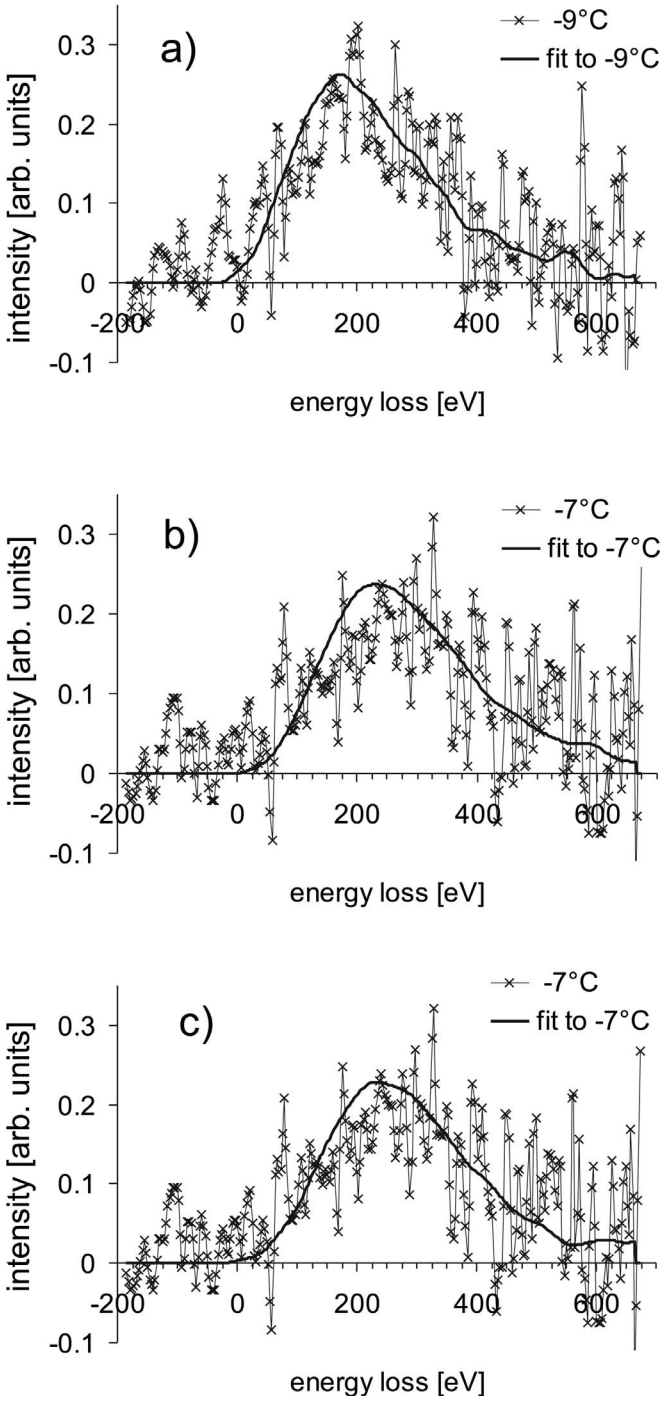

FIG. 5. Fit of the energy loss spectra. The spectra are fitted by consecutively convoluting a spectrum measured at a lower temperature with a function shown in Fig. 6. In (a) and (b) the −13.2 °C spectrum is convoluted, in (c) the −12 °C spectrum is convoluted.

IV. DISCUSSION

NICIS spectra of aqueous solutions of Bu_4NI and LiCl were measured. The density of the gas phase was changed by changing the temperature of the solution in order to determine the mean energy loss and the energy loss straggling for helium projectiles with a kinetic energy of 3 keV in water vapor. The mean energy loss in the gas phase was determined

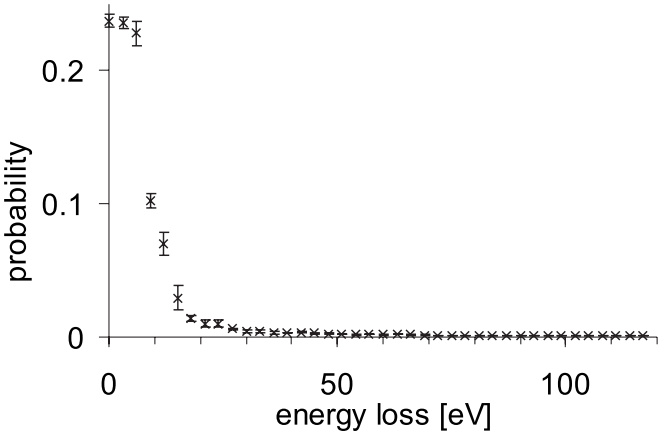

FIG. 6. Energy loss distribution for a mean energy loss of 8.3 eV (single layer). The curve is a weighted average of four different curves each used to convolute the spectra at −13.2 °C, −12 °C, −10.5 °C, and −9 °C to fit the spectra measured at the higher temperature than the convoluted spectrum. The error bars are calculated from the differences between the four curves.

from the shift of the center of gravity. The energy loss straggling was determined from the broadening of the iodide peak in the energy loss spectra. In the data evaluation it was assumed that the shape of the concentration depth profiles does not significantly change upon changing the temperature. The assumption seems to be reasonable since no significant changes were observed in the shape of the concentration depth profiles of Bu_4NI or similar surfactants in solutions with formamide as solvent by changing the temperature of the solutions by several Kelvin.

The accuracy of the energy loss distribution in a single layer is crucial for the deconvolution of the spectra described below. The error bars of the energy loss distribution in a single layer as shown in Fig. 6 are small. Thus it can be concluded that the accuracy in determining the energy loss distribution in a single layer is good.

The energy loss distribution describes all effects that cause the broadening of the energy distribution of the projectiles: multiple small angle scattering, the electronic energy loss straggling and the blurring of the backscattering angle. However, in the energy loss distribution shown here the last contribution is small compared to the other two. In Fig. 8 the full-width at half-maximum (FWHM) of the distribution of the backscattering angle is shown as a function of the total energy loss in the gas phase calculated with SRIM 2003 [41]. Additionally, the broadening of the energy distribution due to the blurring of the backscattering angle is shown. It can be seen that this contribution to the width of the distributions as shown in Fig. 7 is small and can be neglected.

The knowledge of the energy loss straggling distribution makes a further important step in the data evaluation possible. The energy loss straggling distribution can be used to deconvolute the iodide spectra. For the deconvolution, the distribution of inelastic energy losses of the projectiles during the backscattering process also must be known as well as the distribution of kinetic energies of the primary ions. The distribution, taking into account both single distributions, was measured by gas phase experiments [14]. The deconvolution was carried out with an algorithm as described in [10]. The deconvolution of the spectrum measured at −13.2 °C was shown in Fig. 9(a) and the concentration depth profile in Fig. 9(b). The zero of the depth scale was determined both from the gas phase spectrum and the shift of the spectra due

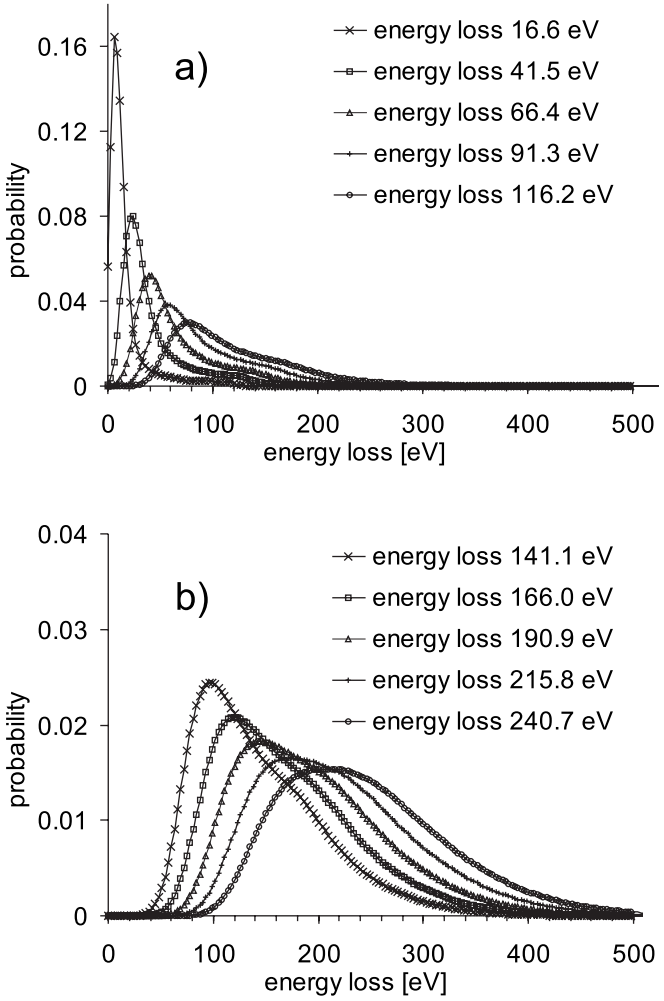

FIG. 7. Energy loss distributions for mean energy losses with a multiple of the mean energy loss in the single layer.

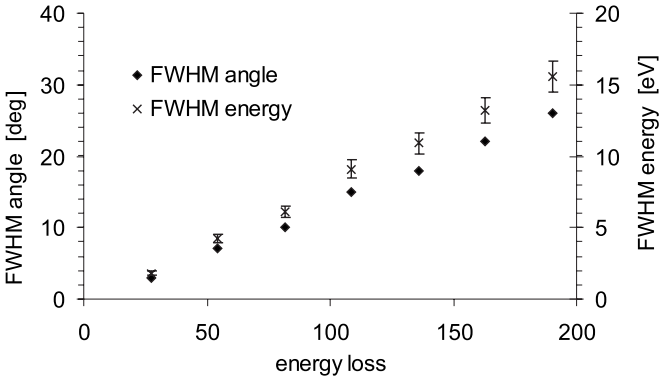

FIG. 8. FWHM of the distribution of the backscattering angle as a function of the energy loss in the water vapor. Additionally the FWHM of the energy distribution caused by the blurring of the backscattering angle is shown.

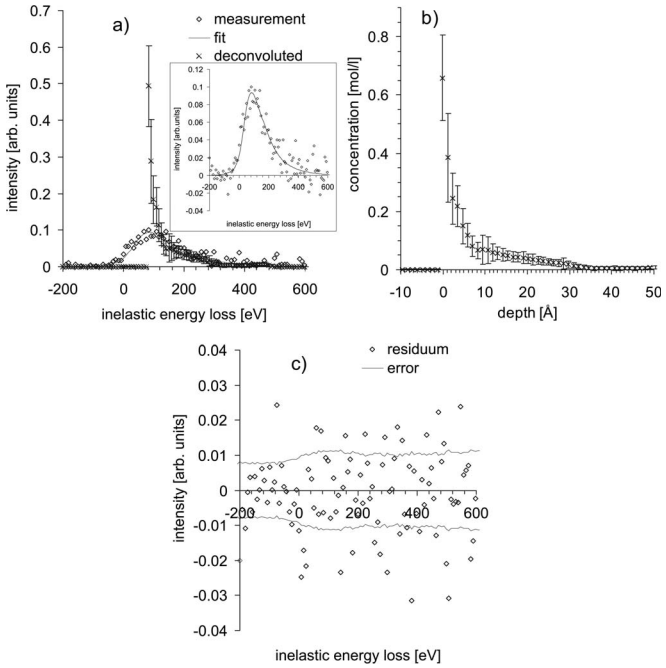

FIG. 9. (a) Energy loss spectrum and deconvoluted energy loss spectrum of iodide of the $0.01m\mathrm{Bu_4NI}$ and $2.5m\mathrm{LiCl}$ solution in water at −13.2 °C, (b) concentration depth profile based on the deconvolution of the energy loss spectrum, (c) the residuum with the experimental error. The inset in (a) shows the experimental spectrum and the fit which is the convolution of the deconvoluted energy loss spectrum. The surface excess of iodide is $(4\pm0.5)\times10^{-11}$ mol/cm^2.

to the presence of the gas phase in front of the target as shown in Fig. 4. In the inset of Fig. 9(a) the measured and fitted spectra are shown. In Fig. 9(c) the residuum is shown. Both figures demonstrate the accuracy of the fit. The deconvoluted spectra measured at −12 °C and −10.5 °C result in concentration depth profiles of the iodide that are the same as the one in Fig. 9(b) within the error bars. The error bars in Fig. 9(b) are calculated from the statistics of the algorithm reflecting the variety of the deconvoluted concentration depth profiles, that describe the measurement equally well. The concentration depth profile of iodide in Fig. 9(a) shows a strong enrichment of the iodide at the surface in a thin layer. This is expected as Bu_4N^+ will adsorb at aqueous surfaces due to the four butyl groups. Due to the demand of charge equilibrium there must be also an adsorption of counter ions. Since iodide has a greater ionic radius than chloride it can be expected that the major fraction of the counter ions equalizing the charge of the Bu_4N^+ will consist of iodide rather than of chloride. The concentration of iodide drops sharply to a low concentration below the surface followed by a gradual drop to the bulk concentration within several Å. This region is commonly called the diffusive layer. The details of the concentration depth profiles in the diffuse layer depend on the accuracy of the fitting of the energy loss distribution.

V. CONCLUSION AND OUTLOOK

NICIS spectra of an aqueous solution of $0.01m\mathrm{Bu_4NI}$ and $2.5m\mathrm{LiCl}$ are measured at different temperatures. The energy loss spectra of iodide show a shift of the maximum and a broadening. By fitting the spectra quantitatively both the energy loss of the projectiles in the gas phase and the energy loss distribution could be determined. This information can be used to deconvolute the energy loss spectra and to determine concentration depth profiles. The iodide in the aqueous solution adsorbs strongly at the surface within a layer of a few Å. The method described here will be used to determine concentration depth profiles of inorganic salts in aqueous solutions.

ACKNOWLEDGMENTS

The author thanks H. Morgner for fruitful discussions and Hartwig Pohl for his contribution in setting up the experiments. The author also acknowledges the support of the German Science Foundation (DFG, Grant No. Mo 288/34).

[1] M. L. Schlossman, Curr. Opin. Colloid Interface Sci. **7**, 235 (2002).
[2] J. R. Lu, R. K. Thomas, and J. Penfold, Adv. Colloid Interface Sci. **84**, 143 (2000).
[3] J. Eastoe, A. Rankin, R. Wat, and C. D. Bain, Int. Rev. Phys. Chem. **20**, 357 (2001).
[4] D. M. Colegate and C. D. Bain, Phys. Rev. Lett. **95**, 198302 (2005).
[5] Y. R. Shen, Pure Appl. Chem. **73**, 1589 (2001).
[6] G. L. Richmond, Chem. Rev. (Washington, D.C.) **102**, 2693 (2002).
[7] G. M. Nathanson, Annu. Rev. Phys. Chem. **55**, 231 (2004).
[8] F. Eschen, M. Heyerhoff, H. Morgner, and J. Vogt, J. Phys.: Condens. Matter **7**, 1961 (1995).
[9] H. Morgner, Adv. At., Mol., Opt. Phys. **42**, 387 (2000).
[10] G. Andersson and H. Morgner, Surf. Sci. **445**, 89 (2000).
[11] E. Kührt and R. Wedell, Phys. Lett. **96A**, 347 (1983).
[12] E. Szilágyi, Nucl. Instrum. Methods Phys. Res. B **161-163**, 37 (2000).
[13] M. A. Briere and J. P. Biersack, Nucl. Instrum. Methods Phys. Res. B **64**, 693 (1992).
[14] G. Andersson, H. Morgner, and K.-D. Schulze, Nucl. Instrum. Methods Phys. Res. B **190**, 222 (2002).
[15] D. L. Mason, R. Prior, and A. R. Quinton, Nucl. Instrum. Methods **45**, 41 (1966).
[16] K. W. Kemper, D. Haynes, and N. Fletcher, Nucl. Instrum. Methods **88**, 289 (1970).
[17] B. Efken, D. Hahn, D. Hilscher, and G. Wüstefeld, Nucl. Instrum. Methods **129**, 219 (1977).
[18] H. Bichsel, Phys. Rev. A **9**, 571 (1974).
[19] L. D. Landau, J. Phys. (USSR) **8**, 201 (1944); L. D. Landau, *Collected Papers*, edited by D. ter Haar (Pergamon, Oxford, 1965), p. 471.
[20] P. V. Vavilov, Sov. Phys. JETP **5**, 749 (1957).

[21] M. S. Livingston and H. Bethe, Rev. Mod. Phys. **9**, 245 (1937).
[22] V. Martini, Nucl. Instrum. Methods **124**, 119 (1975).
[23] C. Garrett, Science **303**, 1146 (2004).
[24] P. Jungwirth and D. Tobias, Chem. Rev. (Washington, D.C.) **106**, 1259 (2006).
[25] P. Petersen and R. Saykally, Chem. Phys. Lett. **397**, 51 (2004).
[26] D. Liu, G. Ma, L. Levering, and H. Allen, J. Phys. Chem. B **108**, 2252 (2004).
[27] S. Ghosal, J. C. Hemminger, H. Bluhm, B. S. Mun, E. L. D. Hebenstreit, G. Ketteler, D. F. Ogletree, F. G. Requejo, and M. Salmeron, Science **307**, 563 (2005).
[28] D. F. Ogletree, H. Bluhm, G. Lebedev, C. S. Fadley, Z. Hussain, and M. Salmeron, Rev. Sci. Instrum. **73**, 3872 (2002).
[29] G. Andersson and H. Morgner, Surf. Sci. **405**, 138 (1998).
[30] G. Andersson, H. Morgner, and H. Pohl (unpublished).
[31] K. Scheel and W. Heuse, Ann. Phys. **29**, 723 (1909).
[32] L. Rayleigh, Z. Phys. Chem., Stoechiom. Verwandtschaftsl. **37**, 713 (1901).
[33] *CRC Handbook of Chemistry and Physics*, 67th ed. (CRC Press, Boca Raton, FL, 1986), p. D. 235.
[34] G. Andersson, T. Krebs, and H. Morgner, Phys. Chem. Chem. Phys. **7**, 136 (2005).
[35] P. Jungwirth and D. Tobias, J. Phys. Chem. B **105**, 10468 (2001).
[36] W. Bragg and R. Kleeman, Philos. Mag. **10**, 318 (1905).
[37] J. Ziegler, *Helium Stopping Powers and Ranges in all Elements* (Pergamon Press, New York, 1977).
[38] E. Szilágyi and F. Pászti, Nucl. Instrum. Methods Phys. Res. B **85**, 616 (1994).
[39] B. Hartmann, S. Kalbitzer, and C. Klatt, Nucl. Instrum. Methods Phys. Res. B **124**, 490 (1997).
[40] N. Matsunami and K. Kitoh, Nucl. Instrum. Methods Phys. Res. B **85**, 556 (1994).
[41] http://www.srim.org/